Supplementary Information for

Assessing Microbial Competition in a Hydrogen-Based Membrane Biofilm Reactor (MBfR) using Multidimensional Modeling

Kelly J. Martin[a,c] , Cristian Picioreanu[b], Robert Nerenberg[a]

[a] Department of Civil and Environmental Engineering and Earth Sciences, University of Notre Dame, 156 Fitzpatrick Hall, Notre Dame, IN 46556, USA

[b] Department of Biotechnology, Faculty of Applied Sciences, Delft University of Technology, Julianalaan 67, 2628 BC Delft, The Netherlands

[c] Current address: Department of Civil and Environmental Engineering, University of Michigan, 1351 Beal Avenue, EWRE 219, Ann Arbor, MI 48109, USA

martinkj@umich.edu

C.Picioreanu@tudelft.nl

nerenberg.1@nd.edu (corresponding author)

+001-574-631-4098 (telephone)

+001-574-631-9236 (fax)

S1. Supplementary information for model definitions

The tables and figure in this section supplement the one- and two-dimensional (1-d and 2-d) model descriptions provided in the manuscript. Please refer to the manuscript for more context.

Table SI: Redox reactions for modeled metabolisms. The reactions are given without consideration of biomass synthesis.

process	redox reaction	ΔG°'(kJ/e^- eq.)
denitrification	$\frac{1}{2}H_2 + \frac{1}{5}NO_3^- + \frac{1}{5}H^+ \rightarrow \frac{1}{10}N_2 + \frac{3}{5}H_2O$	-112
sulfate-reduction	$\frac{1}{2}H_2 + \frac{1}{8}SO_4^{-2} + \frac{3}{16}H^+ \rightarrow \frac{1}{16}H_2S + \frac{1}{16}HS^- + \frac{3}{5}H_2O$	-19
methanogenesis	$\frac{1}{2}H_2 + \frac{1}{8}CO_2 \rightarrow \frac{1}{8}CH_4 + \frac{1}{4}H_2O$	-16

Table SII: Kinetic parameters for the processes given in Table 1 in the manuscript.

Parameter	Symbol	Value	Unit	Reference
Kinetic parameters for denitrifying bacteria				
maximum specific growth rate	$\mu_{max,DN}$	1.28	d^{-1}	based on theoretical stoichiometry; (Rittmann and McCarty, 2001)
decay rate	b_{DN}	0.05	d^{-1}	(Rittmann and McCarty, 2001)
half saturation constant for hydrogen	$K_{H2,DN}$	0.0018	g $H_2 \cdot m^{-3}$	(Smith et al., 1994)
half saturation constant for nitrate	$K_{NO3,DN}$	0.18	g $N \cdot m^{-3}$	(Kurt et al., 1987)
yield on H_2	Y_{DN}	0.00137	kg $COD \cdot g^{-1}$ H_2	based on theoretical stoichiometry; (Rittmann and McCarty, 2001)
fraction of electrons used for energy	f_e°	0.76	-	based on theoretical stoichiometry; (Rittmann and McCarty, 2001)
Kinetic parameters for sulfate-reducing bacteria				
maximum rate of biomass growth	$\mu_{max,SR}$	0.217	d^{-1}	based on theoretical stoichiometry; (Rittmann and McCarty, 2001)
decay rate	b_{SR}	0.05	d^{-1}	used for this study
half saturation constant for hydrogen	$K_{H2,SR}$	0.0016	g $H_2 \cdot m^{-3}$	(Kalyuzhnyi et al., 1998; Kalyuzhnyi and Fedorovich, 1998)
half saturation constant for sulfate	$K_{SO4,SR}$	0.90	g $S \cdot m^{-3}$	(Kalyuzhnyi et al., 1998; Kalyuzhnyi and Fedorovich, 1998)
yield on H_2	Y_{SR}	0.00029	kg $COD \cdot g^{-1}$ H_2	based on theoretical stoichiometry; (Rittmann and McCarty, 2001)
fraction of electrons used for energy	f_e°	0.95	-	based on theoretical stoichiometry; (Rittmann and McCarty, 2001)
Kinetic parameters for methanogens				
maximum rate of substrate utilization	$\mu_{max,MT}$	0.186	d^{-1}	based on theoretical stoichiometry; (Rittmann and McCarty, 2001)
decay rate	b_{MT}	0.05	d^{-1}	used for this study
half saturation constant for hydrogen	$K_{H2,MT}$	0.004	g $H_2 \cdot m^{-3}$	(Kalyuzhnyi et al., 1998; Kalyuzhnyi and Fedorovich, 1998)
half saturation constant for carbon dioxide	$K_{CO2,MT}$	0.12	g $C \cdot m^{-3}$	(Kalyuzhnyi, 1997)
yield on H_2	Y_{MT}	0.00025	kg $COD \cdot g^{-1}$ H_2	based on theoretical stoichiometry; (Rittmann and McCarty, 2001)
fraction of electrons used for energy	f_e°	0.96	-	based on theoretical stoichiometry; (Rittmann and McCarty, 2001)

Table SIII: Physical parameters of the 1-d model.

Parameter	Symbol	Value	Unit	Reference
diffusion coefficient of hydrogen in water	D_{H2}	$0.442 \cdot 10^{-3}$	$m^2 \cdot d^{-1}$ (@25°C)	(Haynes, 2012)
diffusion coefficient of nitrate in water	D_{NO3}	$0.164 \cdot 10^{-3}$	$m^2 \cdot d^{-1}$ (@25°C)	(Haynes, 2012)
diffusion coefficient of sulfate in water	D_{SO4}	$0.092 \cdot 10^{-3}$	$m^2 \cdot d^{-1}$ (@25°C)	(Haynes, 2012)
diffusion coefficient of hydrogen sulfide in water	D_{H2S}	$0.118 \cdot 10^{-3}$	$m^2 \cdot d^{-1}$ (@25°C)	(Haynes, 2012)
diffusion coefficient of hydrogen sulfide ion in water	D_{HS}	$0.149 \cdot 10^{-3}$	$m^2 \cdot d^{-1}$ (@25°C)	(Haynes, 2012)
diffusion coefficient of carbon dioxide in water	D_{CO2}	$0.165 \cdot 10^{-3}$	$m^2 \cdot d^{-1}$ (@25°C)	(Haynes, 2012)
diffusion coefficient of bicarbonate in water	D_{HCO3}	$0.102 \cdot 10^{-3}$	$m^2 \cdot d^{-1}$ (@25°C)	(Haynes, 2012)
diffusion coefficient of carbonate in water	D_{CO3}	$0.080 \cdot 10^{-3}$	$m^2 \cdot d^{-1}$ (@25°C)	(Haynes, 2012)
diffusion coefficient of methane in water	D_{CH4}	$0.129 \cdot 10^{-3}$	$m^2 \cdot d^{-1}$ (@25°C)	(Haynes, 2012)
diffusion coefficient of protons in water	D_H	$0.804 \cdot 10^{-3}$	$m^2 \cdot d^{-1}$ (@25°C)	(Haynes, 2012)
diffusion coefficient of hydroxide in water	D_{OH}	$0.129 \cdot 10^{-3}$	$m^2 \cdot d^{-1}$ (@25°C)	(Haynes, 2012)
ratio of diffusion in biofilm/diffusion in water	ψ_d	0.8	-	(Rittmann and McCarty, 2001)
Henry's Law constant	H_{H2}	0.64	$m^3\ atm \cdot g^{-1}\ H_2$	(Haynes, 2012)

For the 1-d model, the concentration of dissolved components in the bulk liquid and membrane lumen were assumed constant in time and space. This explains the very high influent flowrates into the bulk liquid $Q_{in\ bl}$ and lumen $Q_{in,mem}$, relative to the volume of the biofilm V_{bio} and lumen V_{lumen} and rates of transformation. The choice in biofilm surface area became inconsequential with the simulation of constant concentrations, though the ratio of inner biofilm area A_{inner} to outer biofilm area A_{outer} was important (see Section 3.3 in the manuscript). For a flat attachment surface, the ratio A_{inner}:A_{outer} = 1. Table SIV also lists the diffusivity D_{mem} and thickness of the membrane t_{mem}, which were pertinent to hydrogen mass transport into the biofilm.

Table SIV: Program parameters for the 1-d model.

Parameter	Symbol	Value	Unit	Reference
attachment surface area	A_{inner}	0.025	m^2	chosen for this study
outer biofilm surface area	A_{outer}	0.025	m^2	chosen for this study
volume of biofilm compartment	V_{bio}	1	m^3	chosen for this study
volume of lumen	V_{lumen}	1	m^3	chosen for this study
influent bulk liquid flowrate	$Q_{in,bl}$	1000	$m^3 \cdot d^{-1}$	chosen for this study
influent lumen flowrate	$Q_{in,mem}$	1000	$m^3 \cdot d^{-1}$	chosen for this study
diffusivity of membrane material	D_{mem}	$5.5 \cdot 10^{-6}$	$m^2 \cdot d^{-1}$	chosen for this study
thickness of membrane	t_{mem}	$50 \cdot 10^{-6}$	M	chosen for this study
biomass density	ρ_X	112	kg COD$\cdot m^{-3}$	chosen for this study (see section S2)
liquid fraction	ε_l	0.8	-	chosen for this study
liquid diffusion layer	*LDL*	100	µm	chosen for this study

Figure S1 shows the modeling domain used in the 2-d biofilm model. The gas-supplying hollow fiber membrane fabric was represented at the bottom of the channel.

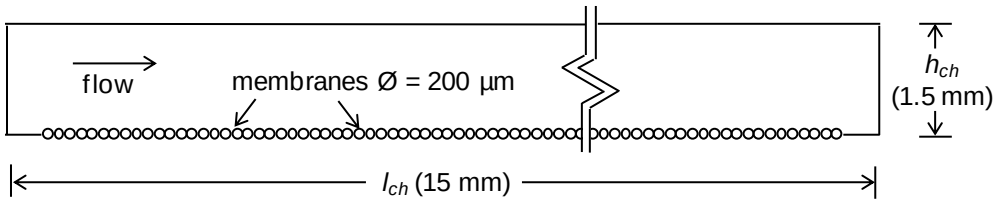

Figure S1: 2-d modeling domain

Table SV: 2-d model parameters. The 2-d model of this study was based on the single species model of Martin et al. (2013) as is referenced in the manuscript. Therefore, the use of some of the listed parameters are not explicitly described in the manuscript, but in Martin et al. (2013).

Parameter	Symbol	Value	Unit	Reference
channel length	l_{ch}	$15 \cdot 10^{-3}$	m	chosen for this study
channel height	h_{ch}	$1.5 \cdot 10^{-3}$	m	chosen for this study
outer diameter of membrane	d_{mem}	$200 \cdot 10^{-6}$	m	chosen for this study
grid dimensions	$\delta x, \delta y, \delta z$	$1 \cdot 10^{-5}$	m	chosen for this study
biomass/bulk maximum triangular mesh size	-	$20 \cdot 10^{-6}/50 \cdot 10^{-6}$	m	chosen for this study
time step	Δt	4	hr	chosen for this study
diffusivity of membrane material	$D_{H2,mem}$	$5.5 \cdot 10^{-6}$	$m^2 \cdot d^{-1}$	chosen for this study
thickness of membrane	t_{mem}	$50 \cdot 10^{-6}$	m	chosen for this study
density of water	P	1000	$g \cdot m^{-3}$	(Haynes, 2012)
dynamic viscosity of water	μ	$1 \cdot 10^{-3}$		((Haynes, 2012)
ratio of diffusion in biofilm/diffusion in water	ψ_d	0.8	-	(Rittmann and McCarty, 2001)
elastic modulus of biofilm	E	64	$N\ m^{-2}$	(Picioreanu et al., 2000)
Poisson's ratio for biofilm	υ_p	0.3	-	(Picioreanu et al., 2000)
threshold stress	σ_{det}	3.0	$N \cdot m^{-2}$	(Picioreanu et al., 2000)
cell density	ρ_X	30	kg $COD \cdot m^{-3}$	(Rittmann and McCarty, 2001)
maximum particle diameter before division	d_{max}	$9 \cdot 10^{-6}$	m	chosen for this study
biomass attachment rate	-	0.005*current # particles	particles	chosen for this study

S2. Matching the 1-d and 2-d model biofilm densities

We want to match the characteristics of the 1-d and 2-d biofilms as best as possible. In Aquasim, the biofilm is divided into a particulate fraction ε_p and a liquid fraction ε_l (i.e., pore space). AQUASIM infers ε_p and ε_l from the user-defined parameters of particulate fraction density ρ_X, and volume-based particulate concentration S_X, knowing $S_X = \varepsilon_p \cdot \rho_X$ and $\varepsilon_p + \varepsilon_l = 1$. AQUASIM also internally calculates effective diffusivities D_{eff} for dissolved components within the biofilm according to $D_{eff} = \varepsilon_l \cdot D_{water}$, where D_{water} is the diffusivity in water.

The 2-d biofilm model assembles rigid, circular biomass entities where all entities touch without overlap. In this case, the maximum achievable particulate fill fraction ε_p is 0.8. In the 2-d model, we define the particulate density ρ_x to equal 30 kg COD·m^{-3}, making S_x = 24 kg COD·m^{-3} (Table SV). In addition, D_{eff} of each component was assigned as 80% of the diffusivity in water, as is commonly used and supported by literature findings (Rittmann and McCarty, 2001). However, based on ε_p = 0.8, AQUASIM internally calculates the effective diffusivity in the 1-d model according to $D_{eff} = 0.2 \cdot D_{water}$. To impose an effective diffusivity of $0.8 \cdot D_{water}$, we defined the ε_p and ε_l fractions as 0.2 and 0.8, respectively, and adjusted ρ_x to be 120 kg COD·m^{-3} (Table SIV). This way, S_x remained as 24 kg COD·m^{-3}. AQUASIM uses the volume-based particulate concentration S_X to calculate the solution, so changes to ε_p and ρ_x do not affect the results.

S3. Effect of hydrogen intramembrane pressure

Experimental MBfR literature stresses the importance of controlling the hydrogen concentration to limit SRB and MET growth (Lu et al., 2009; Ziv-El and Rittmann, 2009). Figure S2 shows the nitrate, sulfate, and methane fluxes for variable sulfate and intramembrane hydrogen pressures at two different biofilm thicknesses. The 100 µm thick biofilm experienced less diffusional resistance, which led to higher rates of denitrification than the 300 µm biofilm (Figure S2a and d). The 100 µm biofilm faced

significant hydrogen limitation at an intramembrane hydrogen pressure of 1.7 atm, restricting rates of denitrification and stopping SRB activity (Figure S2b). Increasing the hydrogen intramembrane pressure improved denitrification, although with diminishing returns. Eventually, the hydrogen pressure no longer limited denitrification and excess hydrogen supported sulfate reduction and methane production, though MET were only active when bulk liquid sulfate concentrations were low (Figure S2b and c). The 300 µm biofilm never experienced significant hydrogen limitation as the nitrate fluxes were very similar at $S_{NO3,bl}$ = 1 g N·m^{-3} for each scenario (Figure S2c). Interestingly, intramembrane hydrogen pressures of 1.7 and 2.7 atm supported slightly greater nitrate fluxes than at an intramembrane pressure of 3.7 atm due to the unique niche created at the inside of the biofilm. At greater hydrogen pressures, substantial SRB and MET concentrations increased near the membrane, where they consumed hydrogen and lowered the rate of hydrogen delivery to the DNB locating in the outer regions of biofilm. The nitrate was still completely consumed within the biofilm, albeit at lower rates. The rates of sulfate reduction and methane production were greater for the 300 µm biofilm as the thicker biofilm introduced greater diffusional resistance for hydrogen and nitrate transport (Figure S2e and f).

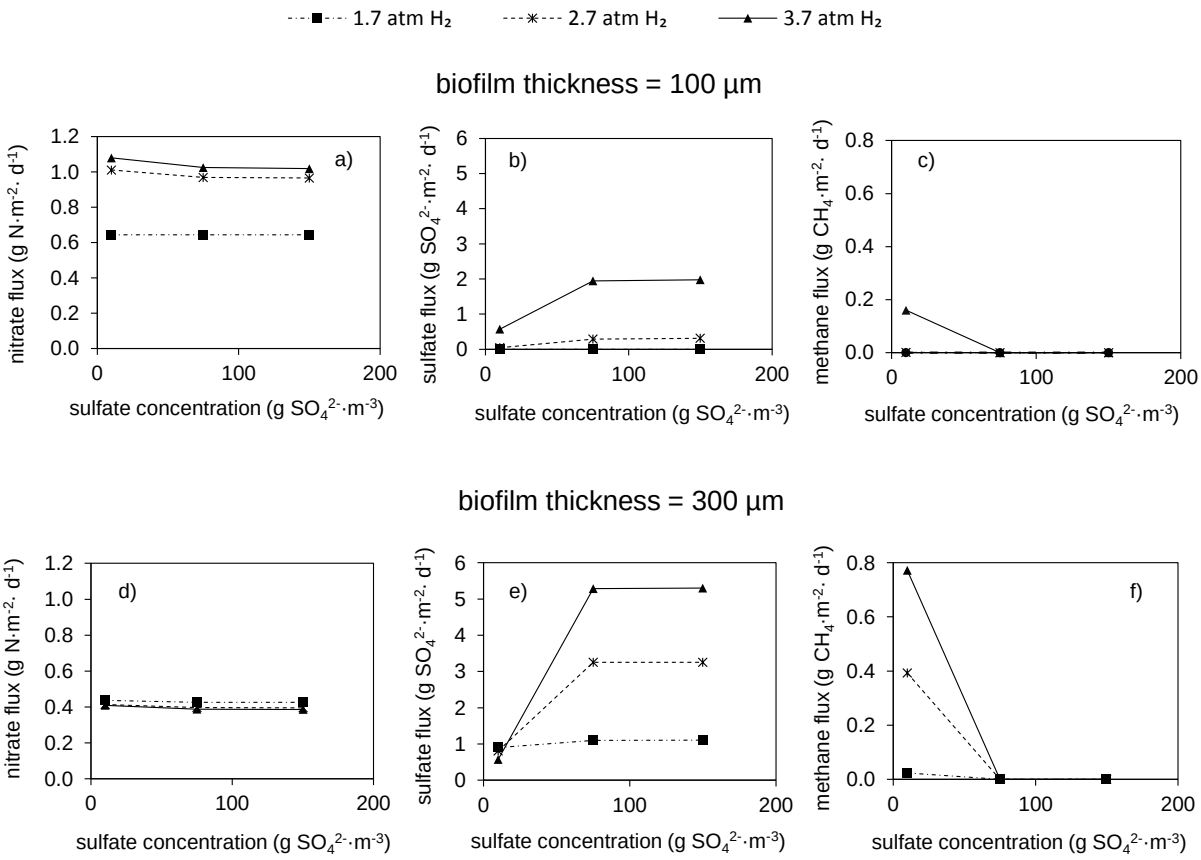

Figure S2: Effect of hydrogen pressure on a) nitrate flux, b) sulfate flux, and c) methane flux as the bulk liquid sulfate concentration was varied for a 100 µm thick biofilm and d) nitrate flux, e) sulfate flux, and f) methane flux for a 300 µm thick biofilm. The bulk liquid nitrate concentration was set to 1 g $N \cdot m^{-3}$.

S4. Substrate profiles for biofilms of variable thickness

See the manuscript, Section 3.1.2. for context for the figure.

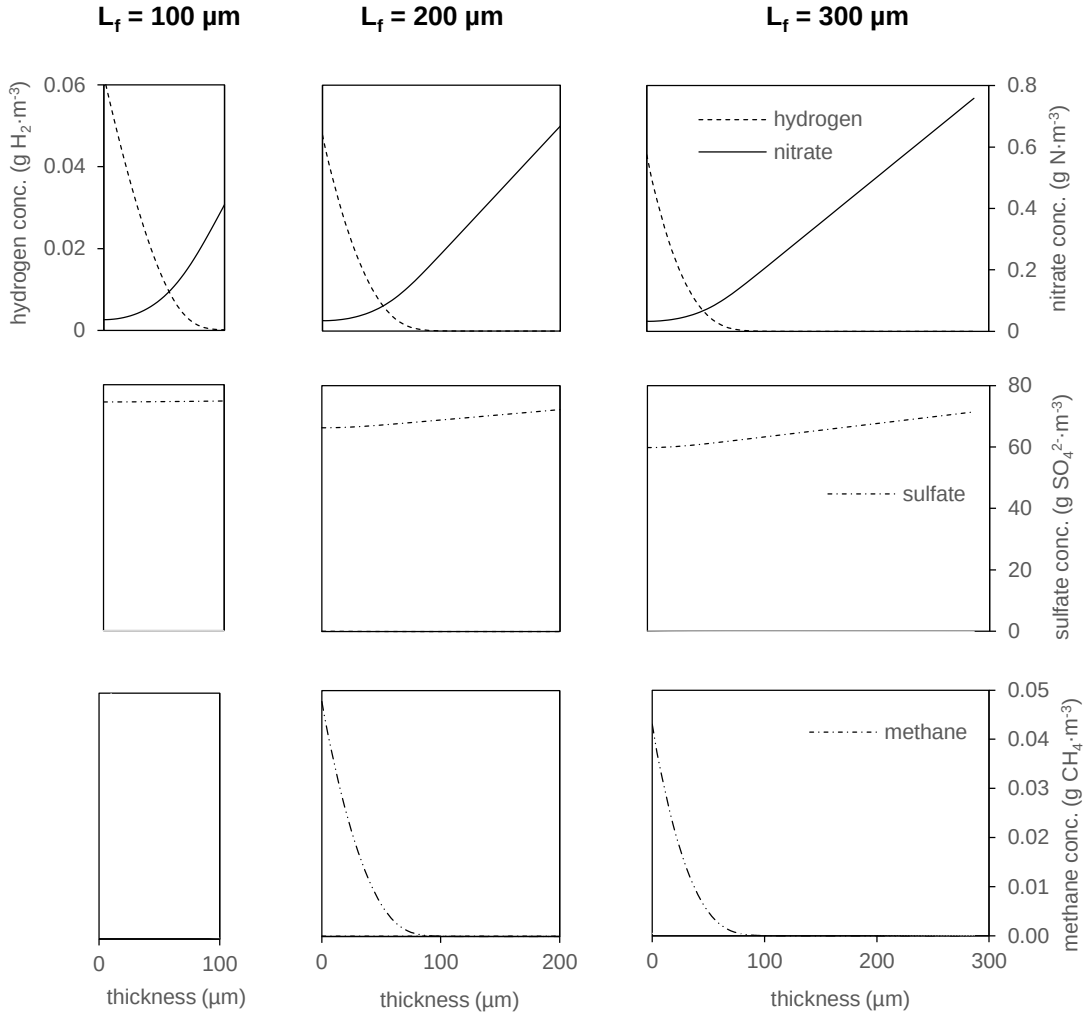

Figure S3: Substrate profiles for biofilms of 100, 200, and 300 µm thickness.

S5. Effect of liquid diffusion layer (LDL) on flux

Formation of preferential flow zones is a common problem in membrane reactors, especially in configurations based on tightly packed membranes (e.g., bundling). With preferential flow, some biofilms will be relegated to zones of stagnation, where diffusion is the main mode of mass transport. These biofilms experience thick LDLs, which lead to a decline in substrate flux. The

effect of the LDL thickness on nitrate and sulfate flux is shown in Figure S4. Nitrate flux decreased with increasing LDL thickness, severely limiting the biofilm of nitrate. Sulfate remained non-limiting, therefore sulfate flux was not impeded. Moreover, with increasing LDL thickness, hydrogen became available to the SRB and improved sulfate flux.

The effect of LDL thickness experienced diminishing returns. Decreasing LDL thickness from 1000 µm to 500 µm exhibited little affect reactor performance, but decreasing it from 500 µm to 300 µm resulted in significant improvements. The LDL had greater effect on the thinner biofilm of 100 µm than the 300 µm biofilm since the 300 µm biofilm was already experiencing the effects of diffusional limitation.

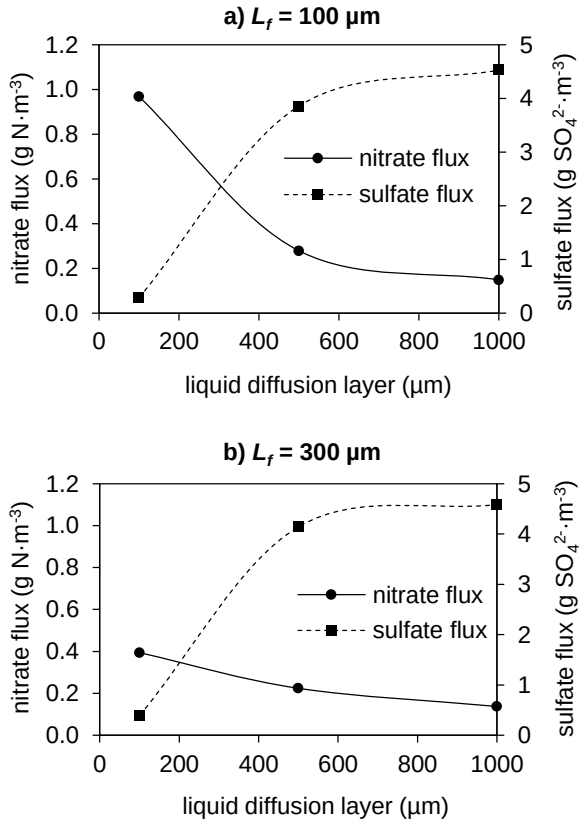

Figure S4: The effect of liquid diffusion layer on the nitrate and sulfate fluxes of a) a 100 µm and b) 300 µm thick biofilm.

S6. References

Haynes WM. 2012. CRC Handbook of Chemistry and Physics 92nd Edition. 92nd ed. Boca Raton, FL.: CRC Press/Taylor and Francis.

Kalyuzhnyi SV. 1997. Batch anarobic digestion of glucose and its mathematical modeling II. Description, verification and application of model. Bioresour. Technol. 59(2):249-258.

Kalyuzhnyi SV, Fedorovich V, Lens P, Po LH, Lettinga G. 1998. Mathematical modelling as a tool to study population dynamics between sulfate reducing and methanogenic bacteria. Biodegradation 9(187-199).

Kalyuzhnyi SV, Fedorovich VV. 1998. Mathematical modelling of competition between sulphate reduction and methanogenesis in anaerobic reactors. Bioresour. Technol. 65(3):227-242.

Kurt M, Dunn IJ, Bourne JR. 1987. Biological denitrification of drinking water using autotrophic organisms with H2 in a fluidized-bed biofilm reactor. Biotechnol. Bioeng. 29(4):493-501.

Lu C, Gu P, He P, Zhang G, Song C. 2009. Characteristics of hydrogenotrophic denitrification in a combined system of gas-permeable membrane and a biofilm reactor. J. Hazard. Mater. 168:1581-1589.

Martin KJ, Picioreanu C, Nerenberg R. 2013. Multidimensional modeling of biofilm development and fluid dynamics in a hydrogen-based membrane biofilm reactor (MBfR). Water Res. 47(13):4739-4751.

Picioreanu C, van Loosdrecht MCM, Heijnen JJ. 2000. Two-Dimensional Model of Bioiflm Detachment Caused by Internal Stress from Liquid Flow. Biotechnol. Bioeng. 72(2):205-218.

Rittmann BE, McCarty PL. 2001. Environmental Biotechnology. Madison, WI: McGraw Hill.

Smith RL, Ceazan ML, Brooks MH. 1994. Autotrophic, hydrogen-oxidizing, denitrifying bacteria in groundwater, potential agents for bioremediation of ntirate contamination. Applied Environmental Microbiology 60(6):1949-1955.

Ziv-El MC, Rittmann BE. 2009. Water quality assessment of groundwater treated with a membrane biofilm reactor. American Water Works Association Journal 101(12):77-83.